Available online at www.sciencedirect.com

ScienceDirect

Advances in Space Research 60 (2017) 796–805

ADVANCES IN SPACE RESEARCH (a COSPAR publication)

www.elsevier.com/locate/asr

Analysis of proton and electron spectra observed by EPT/PROBA-V in the South Atlantic Anomaly

G. López Rosson [a,*], V. Pierrard [a,b]

[a] Royal Belgian Institute for Space Aeronomy (BIRA-IASB), Space Physics, 3 av. Circulaire, B-1180 Brussels, Belgium
[b] Université Catholique de Louvain (UCL), Center for Space Radiations (CSR) and Georges Lemaître Centre for Earth and Climate Research (TECLIM), Earth and Life Institute (ELI), Place Louis Pasteur 3 bte L4.03.08, B-1348 Louvain-La-Neuve, Belgium

Received 29 April 2016; received in revised form 13 March 2017; accepted 16 March 2017
Available online 27 March 2017

Abstract

Proton and electron spectra observed by the Energetic Particle Telescope (EPT) on board the ESA satellite PROBA-V have been investigated at different locations in the South Atlantic Anomaly (SAA). The EPT spectrometer provides high-resolution measurements of the charged particle radiation environment in space performing with direct electron, proton and heavy ion discrimination. Dividing the SAA into 5 different bins of $5° \times 5°$ each one for protons, we obtain that the average proton spectra have often similar slopes, but greatly differ from one location to another. The highest fluxes are generally located in the North of the SAA. For some energy ranges and time periods, the South of the SAA shows different shapes, indicating different sources for the North and South populations of the SAA. Electron spectra show very low fluxes of energetic electrons, often lower than what is provided by the model AE8.

Keywords: South Atlantic Anomaly; Radiation belts; Spectra; EPT

1. Introduction

Proton and electron spectra are often difficult to measure. Electrons can contaminate proton measurements and vice versa. The EPT instrument has been developed to obtain the best discrimination between the particle species and determine precise particle spectra useful for space weather predictions. It was launched on 7 May 2013 to a LEO polar orbit at an altitude of 820 km onboard the ESA satellite PROBA-V with an inclination of 98,73°, a field of view of 52° and 10:30 am as nominal local time at the descending node (Pierrard et al., 2014). The detector measures the particle fluxes for 7 virtual channels for electrons, 11 channels for protons and 11 channels for helium ions. Table 1 summarizes the different energy ranges corresponding to each virtual channel for electrons and protons used in the present study.

EPT can measure up to 10^7 particles/cm^2 s. The detailed characteristics of the instruments are described in Cyamukungu et al. (2014).

Energetic particles are crucial for space engineers to prepare spacecraft missions. The high energy electrons cause a range of problems for satellites like internal satellite charging effects while energetic protons produce cumulative dose and damage as well as prompt Single Event Effects (SEE).

Nevertheless, the present models of space radiation often give very different spectra for the particles, even in stable regions like the inner belt. For instance, the NASA empirical models AP8 (Vette, 1991) and AP9 (Ginet et al., 2013) give very different proton spectra at low altitudes. AP8 is reported to be inadequate as an omnidirectional flux model at highest proton energies (Heynderickx et al., 1999) while AP9 seems inaccurate at low energies (Borisov et al., 2014;

* Corresponding author.
E-mail address: graciela.lopez@aeronomie.be (G. López Rosson).

http://dx.doi.org/10.1016/j.asr.2017.03.022
0273-1177/

Table 1
Energy ranges corresponding to each virtual channel of the EPT instrument for electrons and protons.

Energy channels	Electrons (MeV)	Protons (MeV)
1	0.5–0.6	9.5–13
2	0.6–0.7	13–29
3	0.7–0.8	29–61
4	0.8–1	61–92
5	1–2.4	92–126
6	2.4–8	126–155
7	8–20	155–182
8		182–205
9		205–227
10		227–248
11		>248

Bourdarie et al., 2014). Since EPT can provide accurate measurements and crosses the inner belt in the South Atlantic Anomaly (SAA) at 820 km, it can help to resolve these differences in this region. This is the goal of the present study. Moreover, it was recently shown with Van Allen Probe measurements by Baker et al. (2014) that ultrarelativistic electrons cannot penetrate into the inner belt. Our EPT measurements complete this analysis by providing electron spectra in the SAA and in high latitude regions where the outer belt can penetrate at low altitudes.

2. Spectra in specific bins

To analyze the spectra of protons in the SAA, we have selected 5 bins of 5° × 5° each on different locations inside the SAA.

The different bins are:

- Bin 1: [−50° < Long < −45°], [−25° < Lat < −20°]
- Bin 2: [−35° < Long < −30°], [−25° < Lat < −20°]
- Bin 3: [−50° < Long < −45°], [−40° < Lat < −35°]
- Bin 4: [−35° < Long < −30°], [−35° < Lat < −30°]
- Bin 5: [5° < Long < 10°], [−25° < Lat < −20°]

The bins are illustrated on Fig. 1 for protons in November 2013. The four first bins are located in the heart of the SAA while the fifth bin is more located in its Eastward part. We have chosen these locations in order to compare the possible different populations present there. In all these bins, we calculate the average flux in each energy channel during three months to have enough measures for statistics calculations, and the standard deviation of the mean.

To see better the possible changes of particle fluxes, we have done a zoom on the SAA. If we observe attentively Fig. 2 we can see how the SAA changes depending on the energies. For energies between 13 and 29 MeV (ch2, upper panel) the border of the SAA coincides with L shell $L = 2.2$–2.23, while for higher energy at 155–182 MeV (ch7, bottom panel) the border is now situated at $L = 1.7$–1.73 which means that all the particles between $L = 1.7$ and $L = 2.23$ have disappeared. Note also the region between longitudes -110° and −90°: There are no particles on that region for lower energies, while for ch7 we observe the appearance of particles mainly between −30° latitude to −5°.

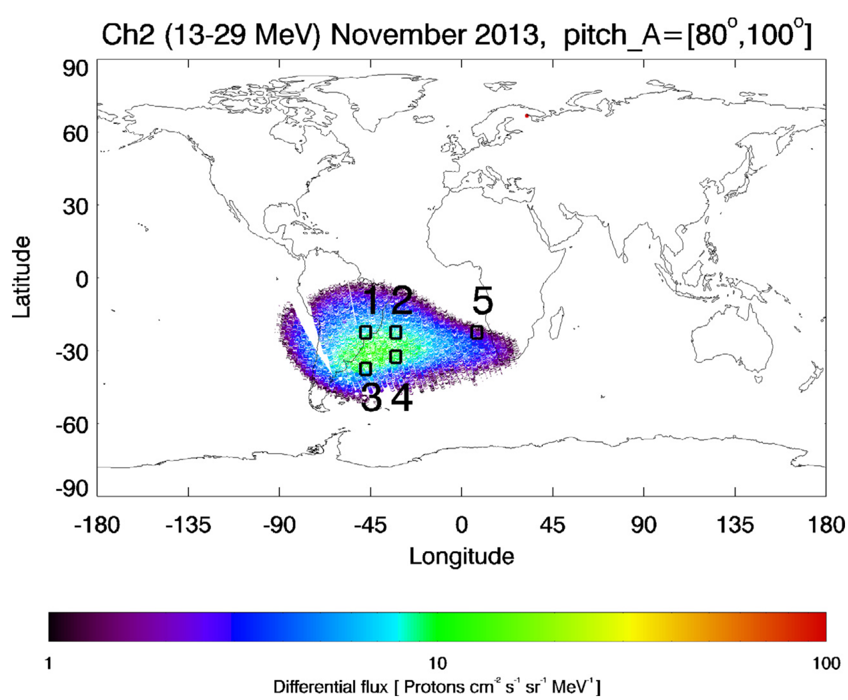

Fig. 1. Proton fluxes measured by EPT in the SAA during November 2013 in channel 2 (13–29 MeV), where all measurements have pitch angles between 80° and 100°. The five bins used for the study are also illustrated.

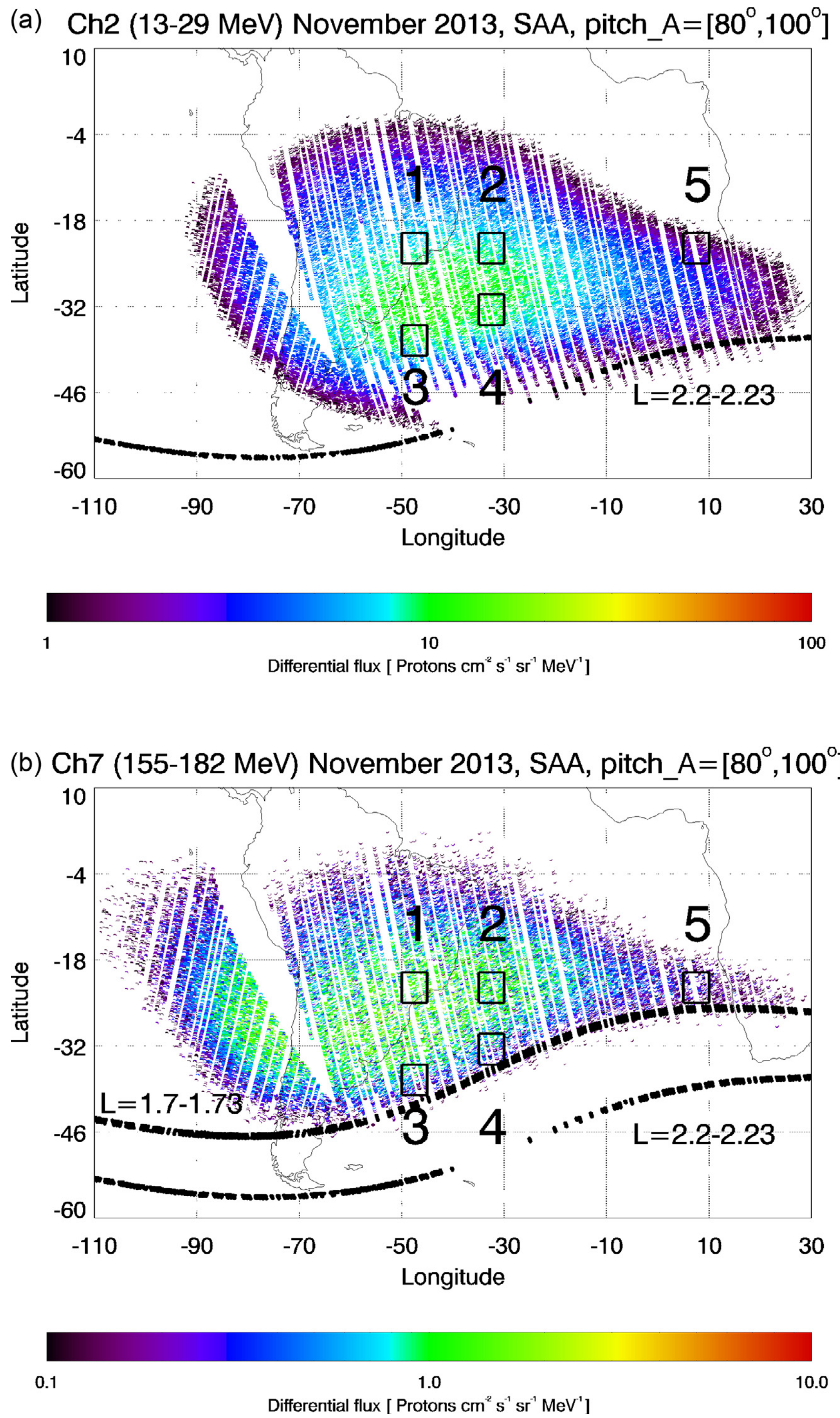

Fig. 2. Zoom of the SAA during November 2013. The upper panel shows channel 2 (13–29 MeV) and the L-shell that crosses the south limit of the SAA. Lower panel shows channel 7 (155–182 MeV) and the L-shells for channel 7 and channel 2. We can see that particles between $L = 2.23$ and $L = 1.7$ have disappeared.

If we take into account that bins 3 and 4 are located almost at the edge of $L = 1.7$ we expect them to have similar spectra.

3. Proton spectra measured by EPT

The proton fluxes measured in the SAA during November 2013 on channel 2 (13–29 MeV) are illustrated on Fig. 1. At the low altitude of 820 km, proton fluxes are only observed in the South Atlantic Anomaly. In case of Solar Energetic Particle (SEP) events, proton fluxes can be also observed at high latitudes during a few days (see Pierrard et al., 2014).

For our study we selected only the observations with pitch angle values between 80° and 100° because it is well known that the proton fluxes measured at low altitudes

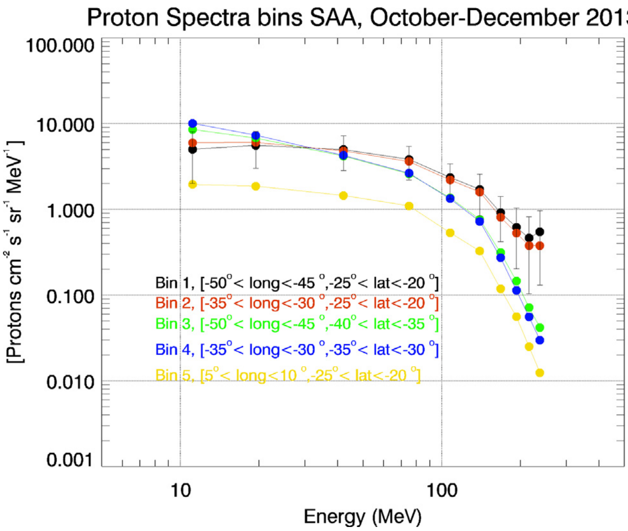

Fig. 3. Average differential proton spectra observed by EPT from October to December 2013 from 9.5 to 248 MeV in the five different bins of the SAA. Error bars are shown for bin 1. The other four bins have similar error bars, but are not shown to avoid confusion.

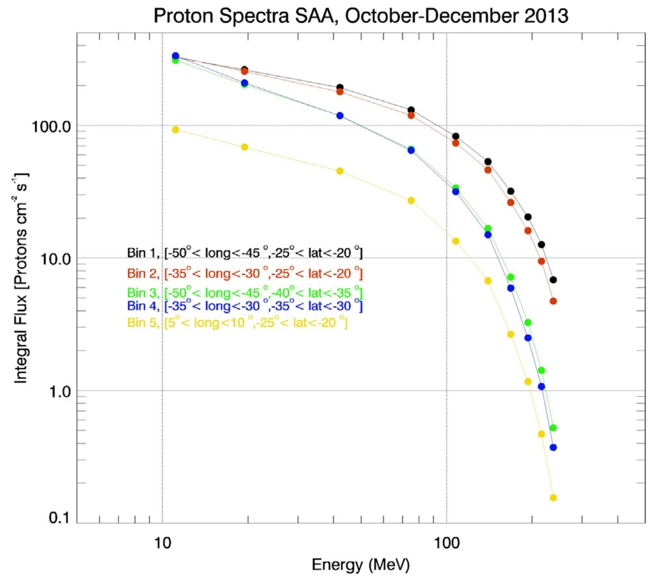

Fig. 4. Same as Fig. 3, but using the integral fluxes.

are highly anisotropic due to the East-West effect (Kruglanski and Lemaire, 1996). We note that the pitch angle selection reduces the extension of the SAA, which is otherwise larger. As it crosses the SAA, the EPT boresight is either towards East during night crossings or towards West during day crossings. Due to the particularity of the PROBA-V orbit, the pitch angle selection makes also appear a triangular empty area over the Pacific Ocean covering also a part of Chile and Argentina. Nevertheless, this selection does not modify the spectra. In the SAA, the proton fluxes are very stable and are not modified from one month to the other, as we will show later.

Fig. 3 illustrates the averaged differential proton spectra in ($\mathrm{cm^{-2}\,s^{-1}\,sr^{-1}\,MeV^{-1}}$) obtained from EPT measurements in each of the 5 selected bins in the SAA during the period between October to December 2013. It may be seen that the spectra have several orders of magnitude difference depending on the location of the bin. These all decrease with energy, but the spectra of bins 3 and 4 (South of SAA) decrease faster than those in bins 1 and 2 (North of SAA). The highest fluxes for lower energies are observed in bins 3 and 4, but for higher energies, bins 1 and 2 have the highest fluxes. Lowest fluxes are obtained in bin 5, in the East of SAA, as we could already expect from the map on Fig. 1. Also notice that the spectra seem to be organized in pairs, possibly related with the bins locations because bin 3 and 4 cross the same L-shell while bin 1 and 2 are close to the same L line ($L = 1.4$–1.6).

This could explain the similarity between each pair of bins.

The different slopes of the differential spectra in the North and the South of the SAA can indicate the presence of two different belts with different origins. The inner belt is assumed to be due to CRAND (Cosmic Ray Albedo Neutron Decay) or to particles of the neutral sheet transported by radial diffusion. Nevertheless, some regions of the inner belt can also be modified during exceptional SEP events as those observed in April 2001 (Boscher et al., 2014).

To study these possible different sources, we have also calculated the omnidirectional integral flux in ($\mathrm{cm^{-2}\,s^{-1}}$) for the five bins, by adding the fluxes observed in the different channels, which is presented on Fig. 4. This time, bins 1 to 4 have practically the same flux for the lowest energy but then they split and we see again the ‘pairs behavior’: same slope and fluxes for bin 1 and 2 while bin 3 and 4 are almost identical. The lowest fluxes again are obtained on bin 5. The different slopes for the integral fluxes in the

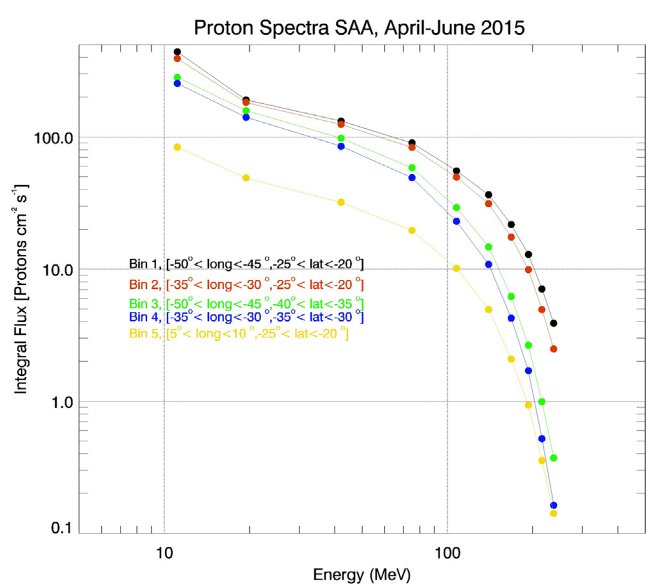

Fig. 5. Averaged proton spectra using integral flux measured by EPT from April to June 2015, for the same five bins used from October to December 2013 in Fig. 4.

North and South parts of the SAA confirm probable different origins.

We have checked the spectra during other periods of time to verify that our results are representative.

Fig. 5 shows the averaged proton spectra using integral fluxes measured by the EPT instrument from April to June 2015. The spectra slopes are almost the same as in October-December 2013, except that the fluxes in bin 1 and 2 have a higher value in 2015. Bin 5 looks identical during both periods. One main difference is that for April-June 2015, the fluxes at the lowest energy channel are different for all the bins, being almost one order of magnitude larger for bins 1 and 2. This may not be satisfactorily explained by the high activity of the year 2015, since the main observed SEP events are observed after April 2015, especially three in June and one in October 2015 (Pierrard and López Rosson, 2016).

During this study we also tested different bin sizes, up to bins of 15° × 15° each on the same locations in the SAA and we obtained similar results on the spectra shapes and flux values.

Fig. 6 shows omnidirectional integral spectra of integral fluxes in ($cm^{-2}\,s^{-1}$) observed in April-June 2015 in bin 1 of the SAA. We have chosen bin 1 because is where we find the highest fluxes. We have compared with the omnidirectional spectra obtained with the empirical models AP8 (Vette, 1991) of NASA for solar minimum and maximum solar activity at a similar position than bin 1 which corresponds to $L = 1.22$–1.25, $B = 0.17$G, using SPENVIS (www.spenvis.oma.be). EPT fluxes are lower than those of the models AP8 MIN and MAX even if we have used the highest fluxes for the comparison. AP8-MAX shows lower fluxes than AP8-MIN at low altitudes because the atmosphere is warmer during maximum solar activity and its expansion at higher altitude erodes more the radiation belts particles trapped in the Earth's magnetic field during this period. The EPT unidirectional differential flux has been converted in omnidirectional integral flux by multiplying it by a factor of 4π but without dividing it by the Badhwar-Konradi scaling factor (Badhwar and Konradi, 1990) depending on the pitch angle distributions of the observations (Borisov et al., 2014).

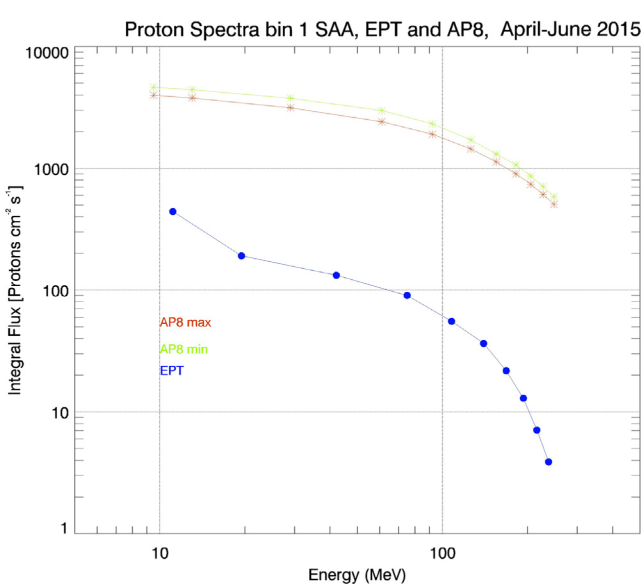

Fig. 6. Average omnidirectional integral proton spectra observed by EPT in April-June 2015 from 9.5 to 248 MeV in bin 1in the SAA, compared with AP8-MIN and AP8-MAX models.

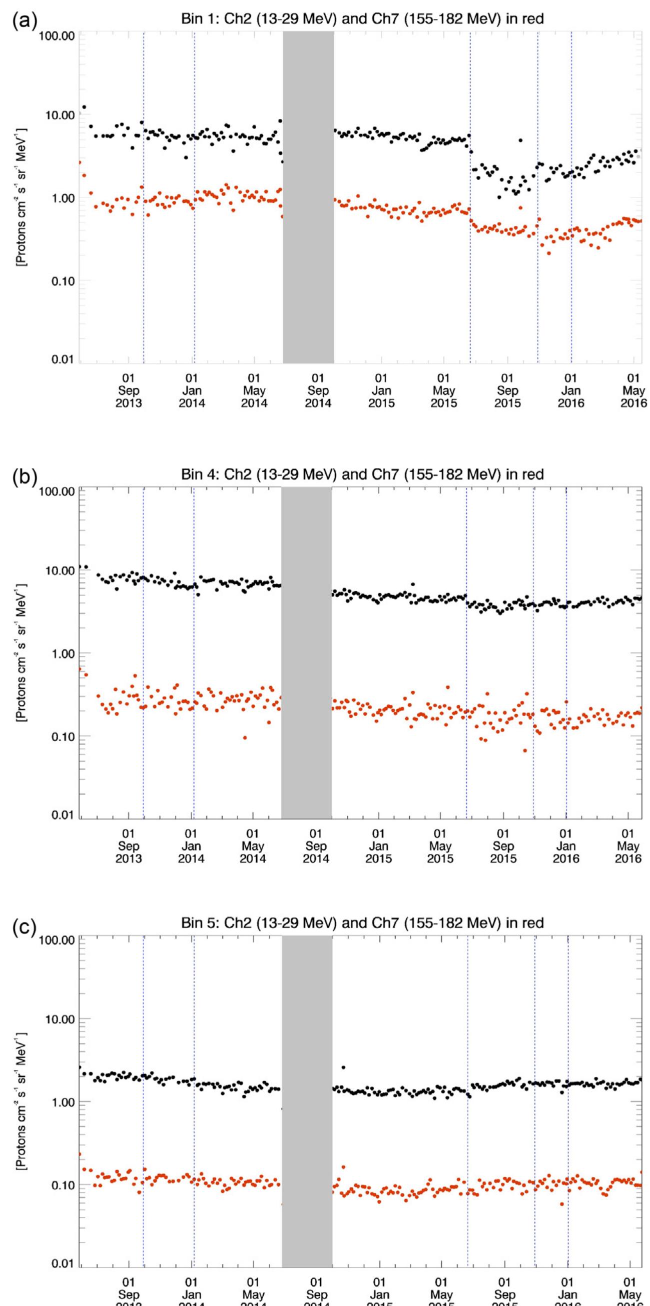

Fig. 7. Temporal evolution of the proton flux during the entire flight period of EPT, for ch2 (13–29 MeV) in black and ch7 (155–182 MeV) in red. Bin 1 is shown on the upper panel, bin 4 in the middle, while bin 5 can be seen on the lower panel. The gray rectangle masks the period when the instrument was off due to calibration. (For interpretation of the references to color in this figure legend, the reader is referred to the web version of this article.)

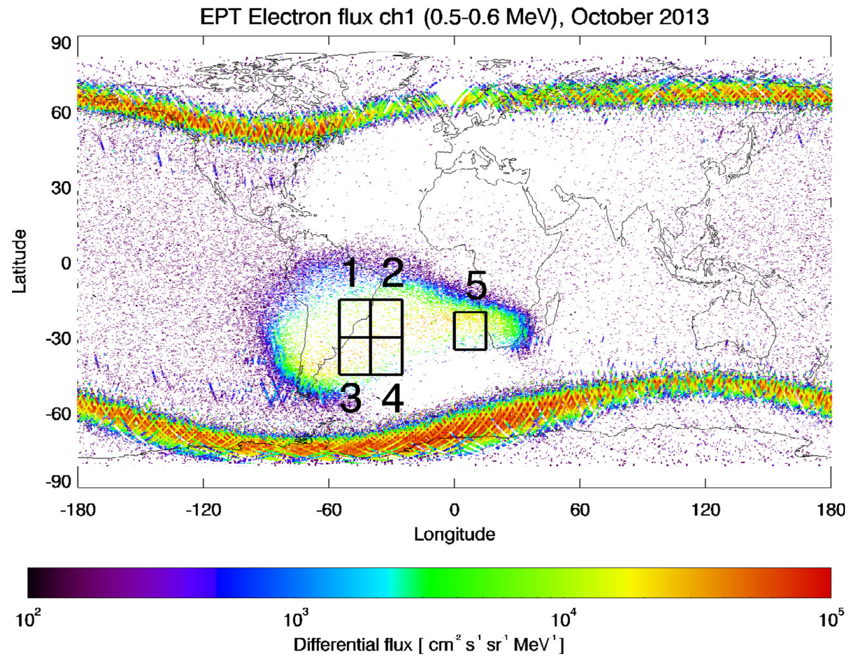

Fig. 8. Map of the electron fluxes in the energy range of 0.5–0.6 MeV (channel 1) observed by EPT during October 2013, showing the five bins that will be studied.

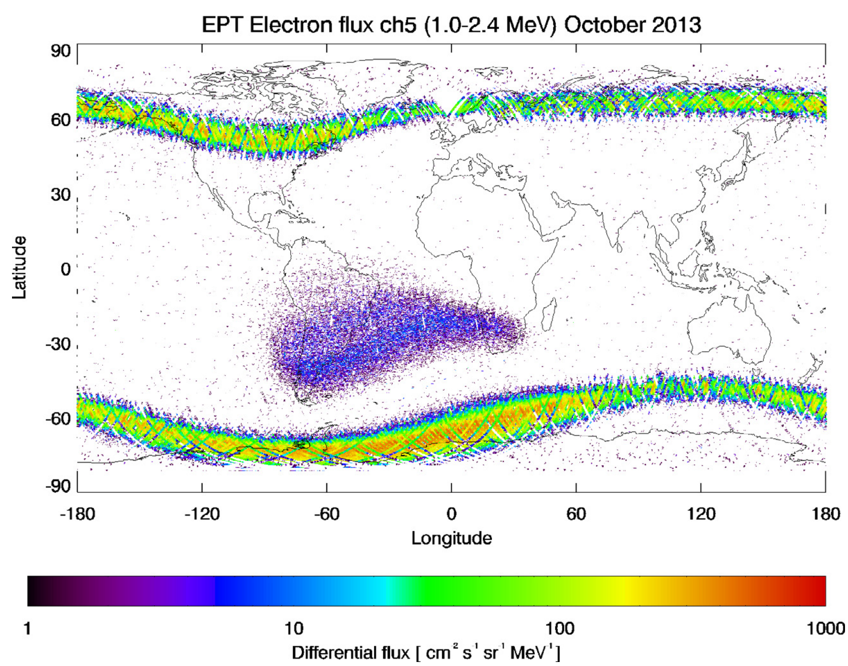

Fig. 9. Map of the electron fluxes in the energy range of 1.0–2.4 MeV (channel 5) observed by EPT during October 2013.

4. Temporal evolution of the flux

Another way to see why the spectra are different and a possible way to prove the existence of two populations is to check the temporal evolution of the flux on the different bins.

Fig. 7 shows the temporal evolution of the proton flux in bins 1, 4 and 5. The gray rectangle covers the dates where the instrument was not working, from June 2014 to September 2014. We have studied the complete flight period of EPT which corresponds to 30 months.

The blue lines on the upper panel show the SEP events (https://umbra.nascom.nasa.gov/SEP/), from left to the right:

1. 30/09/2013
2. 06/01/2014
3. 21/06/2015
4. 29/10/2015
5. 02/01/2016

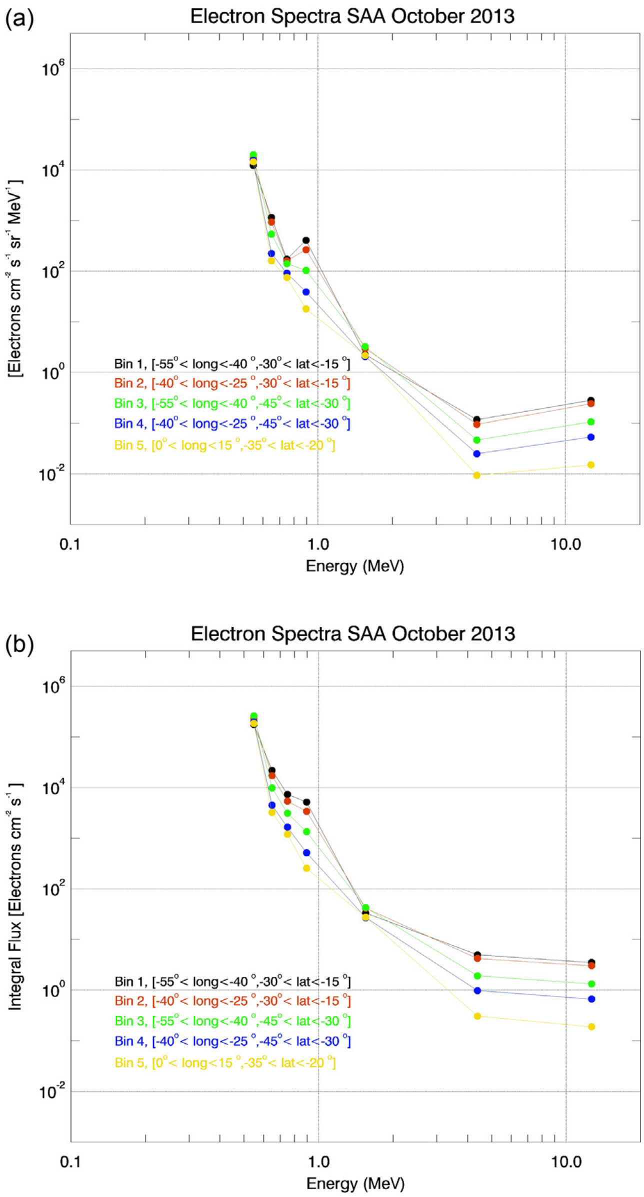

Fig. 10. Average electron spectra observed by EPT in October 2013 in the SAA for the 5 bins color coded. The upper panel shows the differential flux, while the bottom panel shows the integral flux. (For interpretation of the references to color in this figure legend, the reader is referred to the web version of this article.)

All panels of Fig. 7 illustrate fluxes of channel 2 and 7. The fluxes in bin 1 (upper panel) are very variable with time, and show especially a strong decrease after the SEP event of June 2015. The case is similar for bin 2. On the contrary fluxes in bin 4 (middle plot) and bin 5 (see the bottom panel of Fig. 7) show almost no time variations. Results in bin 3 are intermediate, with time variations lower than in bins 1 and 2. From this it is clear that there is one population of protons on the north part of the SAA that changes fast, related with SEP events, but in the south of the SAA there is another population which remains stable during long time periods.

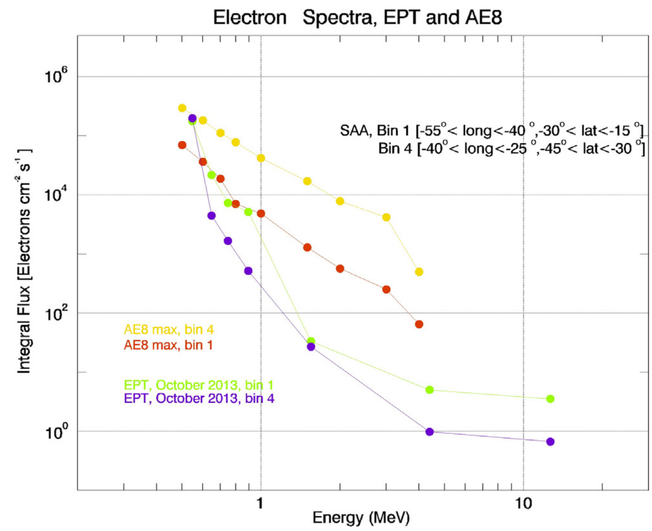

Fig. 11. Average integral electron spectra observed by EPT in October 2013 in bins 1 and 4 of the SAA and comparison with models AE8-MAX on the same bins.

5. Electron spectra in the SAA

The fluxes of electrons in general are very low in the SAA, especially for the energetic electrons and almost zero for ultrarelativistic energies, as recently discovered by Baker et al. (2014).

To study the electron spectra on the SAA, we have taken five bins, located on different regions in the SAA. Note that the shape of the SAA is different for protons and electrons that is why we used different bins:

- Bin 1: [$-55° < \text{Long} < -40°$], [$-30° < \text{Lat} < -15°$]
- Bin 2: [$-40° < \text{Long} < -25°$], [$-30° < \text{Lat} < -15°$]
- Bin 3: [$-55° < \text{Long} < -40°$], [$-45° < \text{Lat} < -30°$]
- Bin 4: [$-40° < \text{Long} < -20°$], [$-45° < \text{Lat} < -30°$]
- Bin 5: [$0° < \text{Long} < 15°$], [$-35° < \text{Lat} < -20°$]

Fig. 8 shows a map of the electron fluxes in the energy range of 0.5–0.6 MeV (channel 1) observed by EPT during the month of October 2013 and the position of the five bins. One can see that the extension of the SAA is a little bit larger than for the protons. In addition to the SAA, fluxes are also observed at high latitudes, corresponding to the penetration of the outer belt at low altitudes.

Fig. 9 shows the electron fluxes in the energy range of 1–2.4 MeV observed by EPT during October 2013. The electron fluxes are very low, especially for larger energies. The shape of the SAA is different from the proton configuration of Fig. 1 and even from the electron SAA at lower energy (see Fig. 8). It is almost empty (very low fluxes) and especially flatter with very low fluxes in the North part of the SAA at this energy range.

The average electron spectra observed by EPT during the month of October 2013 are illustrated on Fig. 10, for the five different bins. The upper figure shows the differen-

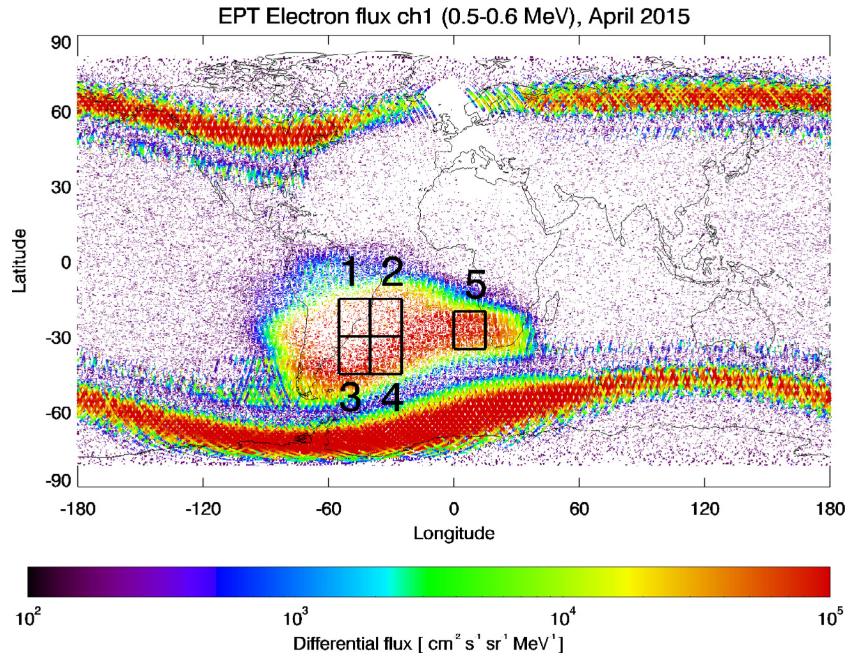

Fig. 12. Same map as Fig. 8, but for April 2015.

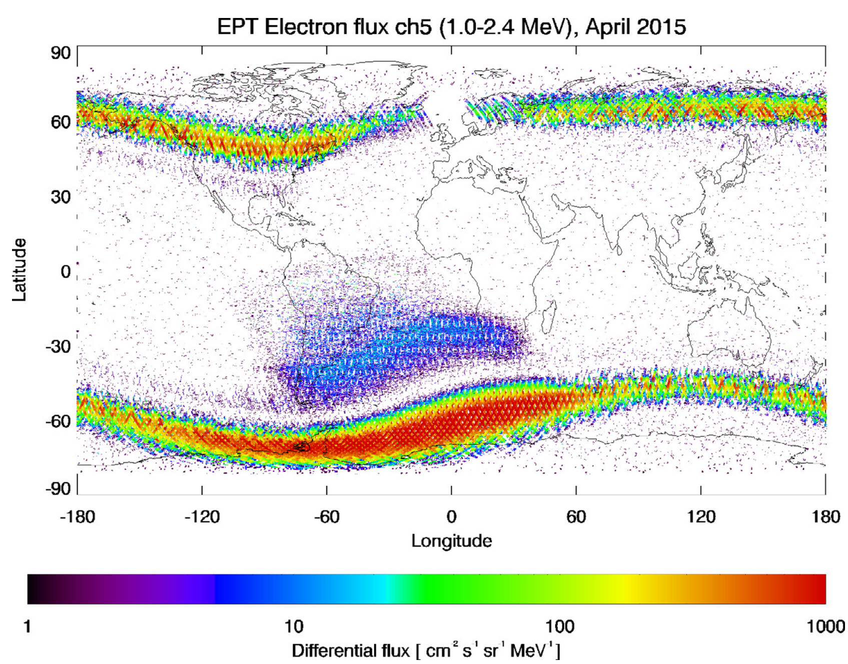

Fig. 13. Map for electrons flux observed by EPT during April 2015 in channel 5 with energies between 1.0 and 2.4 MeV. The fluxes still remain very high in the SAA, mostly in the lower part.

tial flux ($cm^{-2}\,s^{-1}\,sr^{-1}\,MeV^{-1}$) while the bottom panel represents the omnidirectional integral flux ($cm^{-2}\,s^{-1}$). Integral fluxes are always higher since they are calculated by summing up the flux from all energy channels higher than an energy threshold. The differential spectra from Fig. 10 (upper panel) shows clearly a peak in channel 4 (0.8–1 MeV) in bin 1 and 2. Here again, a difference seems to appear between the North and South part of the SAA and the use of differential fluxes instead of integral fluxes allow us to observe these differences and the corresponding energy dependence.

The integral spectra in $cm^{-2}\,s^{-1}$ measured by EPT in October 2013 are compared with the AE8 NASA empirical model (Vette, 1991) in Fig. 11. The model provided by

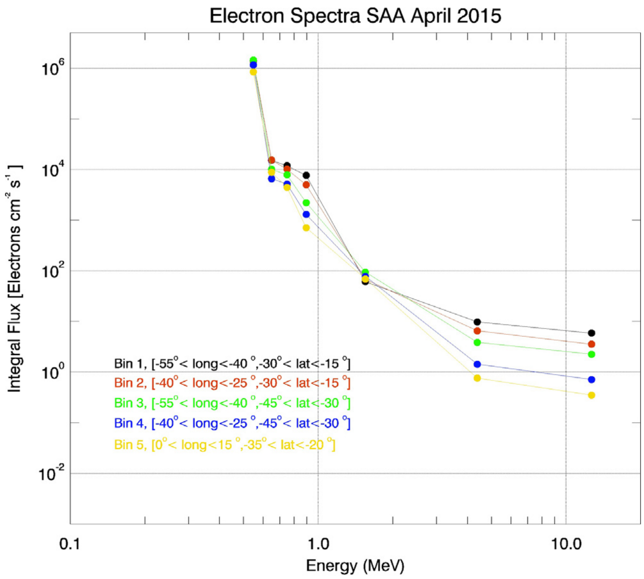

Fig. 14. Omnidirectional integral flux of electrons spectra for the five bins during April 2015.

SPENVIS differentiates minimum and maximum solar activity, but the differences for electron fluxes at 820 km are very small. We used AE8-MAX spectrum because 2013 is close to solar maximum activity.

We have selected two bins to compute the model, at the same locations of EPT bins 1 and 4. In Fig. 11 the yellow[1] curve represents the spectra in bin 4 calculated with AE8 while the red curve is the spectra for bin 1. The difference between both bins predicted by AE8-MAX is higher than the data, where for certain energies the fluxes are practically the same in the two bins, for instance channels 1 and 5.

In the energy region from 0.6 MeV to 1 MeV the fluxes obtained with the NASA model and EPT data are practically the same for bin 1. For other energies, the fluxes observed by EPT in the SAA are lower than the AE8 model.

Models such as AE8 (minimum and maximum) are useful but constructed from relatively sparse datasets, from scientific satellites, and there are large uncertainties over the actual maximum electron flux that might be encountered, its energy spectrum and its duration. That is why EPT measurements with improved particle discrimination can help to improve these models. These fluxes will be used to improve the TOP model especially dedicated to determine dynamical flux variations of electrons at LEO during geomagnetic storms (Benck et al., 2013).

To be sure our spectra are representative, we have also checked the spectra for April 2015, where the five bins on the world map for channel 1 (0.5–0.6 MeV) are shown on Fig. 12.

[1] For interpretation of color in Fig. 11, the reader is referred to the web version of this article.

By comparing Figs. 8 and 12, we may observe that the fluxes are much higher during April 2015, in the outer belt but also in the SAA. This is expected considering the high fluxes measured in 2015 and the intense geomagnetic storms of January and March 2015 (Pierrard and López Rosson, 2016). Note that fluxes remained very high even for higher energies, see for instance Fig. 13 showing the fluxes for channel 5, for energies between 1.0 and 2.4 MeV. But for energies from 2.4 to 8 MeV (Ch6) and above (Ch7), the SAA is almost empty and only high latitude fluxes are observed.

If we look at the spectra shown in Fig. 14, as expected from the information seen on the world maps, the fluxes are higher than in October 2013 (see Fig. 10). For instance for bin 1, the flux in the first channel is higher for more than one order of magnitude in the SAA.

This is a consequence of the big geomagnetic storm occurred on 17th March 2015, where electrons penetrated deep down closer to the Earth, completely filling the slot region and also reaching the inner belt (Pierrard and López Rosson, 2016).

These particles remained trapped for a few weeks after the event, which is why we can observe higher fluxes in April 2015 than in October 2013.

If we compare April 2015 with October 2013, it is visible in Fig. 15 that fluxes are higher by more than one order of magnitude in April 2015 for energies lower than 0.6 MeV. For the other energies, April 2015 shows always higher fluxes than October 2013 but the differences are less significant than in channel 1. Notice that the shapes of the curves are exactly the same for both months.

We have also included the prediction of AE8 for the bin 1. It is clear that this model overestimates electron fluxes for energies higher than 1 MeV.

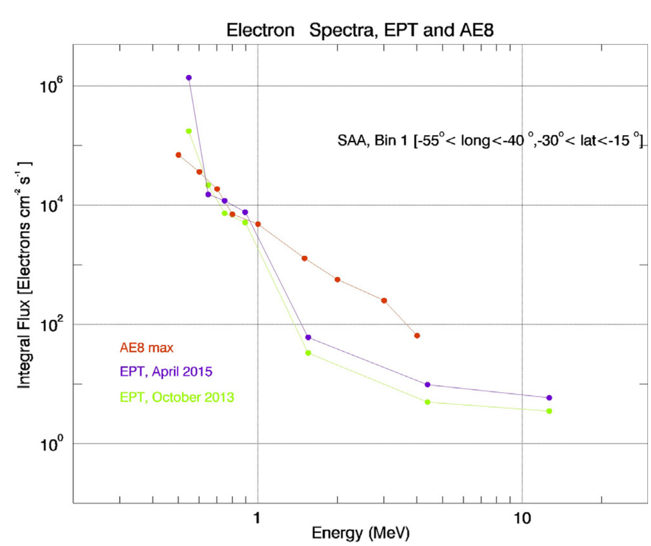

Fig. 15. Average integral electron spectra observed by EPT in October 2013 and April 2015 in bins 1 of the SAA and comparison with predictions for bin 1 of AE8-MAX.

6. Discussion and conclusions

Baker et al. (2014) used Van Allen Probe observation to show that there is an impenetrable barrier to ultrarelativistic electrons at $L < 2.8$ Re so that there is a lack of >2 MeV electrons in the inner belt. With EPT, we study the fluxes in the SAA for $E < 2.4$ MeV and we obtain in general low fluxes of energetic electrons in the SAA, even if they are not completely absent. During the year 2015, higher fluxes are observed in the SAA and they have been injected during geomagnetic storms more than due only to CRAND.

Proton spectra observed by EPT suggest the existence of two different populations of protons in the SAA. One is very stable, with fluxes that remain constant in time, mainly related with CRAND. The other population on the contrary is more variable, on the north part of the SAA where the flux changes can be associated with injection of particles during SEP events, but further study is necessary to understand if there are other physical mechanisms behind this unexpected behavior.

Spectra observed by different instruments can be very different due to the difficulty to discriminate the different particles and possible contaminations of poorly shielded monitors or detectors. The EPT was designed to provide uncontaminated spectra of electrons, protons and alpha particles. The spectra obtained with the EPT in the SAA are compared with empirical models AE8 and AP8. The results show that the AP8 often overestimate the actual unidirectional fluxes when the models of the fluxes are simply divided by 4π, due to flux anisotropy, especially at high energies. Different models (AP8 (Vette, 1991), AP9 (Ginet et al., 2013), CRRESPRO (Meffert and Gussenhoven, 1994)...) also give spectra that can differ by several orders of magnitude in a same location, even for stable regions like in the inner belt. This causes difficulties for engineers when estimating fluxes and radiation doses along orbits of satellites. This is crucial for their security. The spectra provided by EPT can help to improve predictions and to identify sources and loss mechanisms. For the electrons, the fluxes are lower and more stable in the SAA than at high latitudes, but some time variations have been detected, especially associated to geomagnetic storms.

Acknowledgements

The authors thank the Belgian Science Policy – Space Research and Applications for the supplementary researcher program entitled “Scientific analysis of EPT (Energetic Particle Telescope) measurements”. The research leading to these results was also subsidized by the Scientific Federal Policy in the framework of the program Interuniversity Attraction Pole for the project P7/08 CHARM.

The development of the EPT instrument was realized with the support of the Belspo and of the European Space Agency (ESA) (contracts 20294/06/NL/JD (Phase A/B) and 22582/09/NL/AT (Phase C/D)). The design of the EPT instrument and its integration on the PROBA-V satellite results from a fruitful Consortium between the Université Catholique de Louvain (UCL), the Royal Belgian Institute for Space Aeronomy and QinetiQ Space. The B. USOC and the control center in Redu provide data transmission and storage. The Center for Space Radiations at UCL is in charge of the data validation. The authors wish to recognize the contribution of the scientists who participated to the development of the EPT instrument and its integration on PROBA-V satellite. EPT data can be consulted on the website http://csrsrv1.fynu.ucl.ac.be/csr_web/probav/index.html.

References

Badhwar, G.D., Konradi, A., 1990. Conversion of omnidirectional proton fluxes into a pitch angle distribution. J. Spacecraft Rockets 27 (3), 350–352.

Baker, D.N., Jaynes, A.N., Hoxie, V.C., et al., 2014. An impenetrable barrier to ultrarelativistic electrons in the Van Allen radiation belts. Nat. Lett. 515, 531–534. http://dx.doi.org/10.1038/nature13956.

Benck, S., Cyamukungu, M., Cabrera, J., Mazzino, L., Pierrard, V., 2013. The Transient Observation-based Particle (TOP) model and its potential application in radiation effects evaluation. J. Space Weather Space Clim. 3 (A03), 1–10. http://dx.doi.org/10.1051/SWSC/2013024.

Borisov, S., Benck, S., Cyamukungu, M., O'Brien, P., Mazur, J., Nieminen, P., Evans, H., Daly, E., 2014. Angular distribution of protons measured by the energetic particle telescope on PROBA-V. IEEE Trans. 61 (6), 3371–3379. http://dx.doi.org/10.1109/TNS.2014.2361951.

Boscher, D., Cayton, T., Maget, V., et al., 2014. In-flight measurements of radiation environment on board the Argentinean satellite SAC-D. IEEE Trans. Nucl. Sci. 61 (6), 3395–3400. http://dx.doi.org/10.1109/TNS.2014.2365212.

Bourdarie, S., Falguere, D., Inguimbert, C., et al., 2014. Correlation of in-flight displacement damage on the OSL sensor with space environment on-board Jason-2 spacecraft. IEEE Trans. Nucl. Sci. 61 (4), 1643–1647.

Cyamukungu, M., Benck, S., Borisov, S., et al., 2014. The Energetic Particle Telescope (EPT) on board Proba-V: description of a new science-class instrument for particle detection in space. IEEE Trans. Nucl. Sci. 61 (6), 3667–3681. http://dx.doi.org/10.1109/TNS.2014.2361955.

Ginet, G.P., O'Brien, T.P., Huston, S.L., et al., 2013. AE9, AP9 and SPM: new models for specifying the trapped energetic particle and space plasma environment. Space Sci. Rev. 179, 579–615. http://dx.doi.org/10.1007/s1121013-9964-y.

Heynderickx, D., Kruglanski, M., Pierrard, V., et al., 1999. A low altitude trapped proton model for solar minimum conditions based on SAMPEX/PET data. IEEE Trans. Nucl. Sci. 46, 1475–1480.

Kruglanski, M., Lemaire J., 1996. Trapped proton anisotropy at low altitudes, Belgian Institute for Space Aeronomy (BISA), Brussels, Belgium, Tech. Note 6, TREND-3 report.

Meffert, J.D., Gussenhoven, M.S., 1994. CRRESPRO Documentation, PL-TR-94-2218, Environmental Research Papers, 1158, Phillips Laboratory.

Pierrard, V., López Rosson, G., 2016. The effects of the big storm events in the first half of 2015 on the radiation belts observed by EPT/PROBA-V. Ann. Geophys. 34, 75–84. http://dx.doi.org/10.5194/angeo-34-75-2016.

Pierrard, V., López Rosson, G., Borremans, K., et al., 2014. The energetic particle telescope: first results. Space Sci. Rev. 184 (1), 87–106. http://dx.doi.org/10.1007/s11214-014-0097-8.

Vette, J.I., 1991. The AE-8 Trapped Electron Model Environment. NSSDC/WDC-A-R&S, NASA Publication, pp. 91–124.